Modeling and Design of a Voice-Coil Motor for Auto-Focusing Digital Cameras Using an Electromagnetic Simulation Software

Jhih-Da Hsu and Ying-Yu Tzou, *Member, IEEE*

Power Electronics Systems & Chips Lab.
Advanced Power Electronics Center
Department of Electrical and Control Engineering
National Chiao Tung University, Taiwan.

***Abstract*—This paper presents the modeling of a voice coil motor (VCM) used for the auto-focusing control of a digital camera in applications to high-performance mobile phones. The force constant and its associated back EMF constant of a VCM can be highly nonlinear with the mechanical structure. Conventional modeling technique using the derived flux distribution based on geometrical structure is quite involved and impractical to identify its equivalent parameters. A modeling procedure for a specially designed VCM is developed based on its mechanical structure and used material by using an electromagnetic simulation software - the Ansoft's Maxwell 2D. An iterative optimal design process is then proposed to maximize the force constant of the VCM with a specified volume. Simulation results with experimental verification are given to illustrate that the proposed design procedure can achieve a satisfactory performance.**

***Index Terms*—voice coil motor, modeling, electromagnetic simulation, iterative optimal design.**

I. INTRODUCTION

In recent years, mobile phones have been evolved to a development trend to integrate almost every digital media function, such as MP3, voice recorder, digital camera, broadband radio, and even digital TV. At the same time, a mobile phone is also required to be more lighter, thinner, and longer usage time, this means lower power consumption and efficient dynamic power management is a must. Auto-focus is a fundamental requirement for a digital camera or a video recorder. In the conventional approach, the auto-focusing is accomplished via a stepping motor with open-loop control. This solution has disadvantages of low control resolution, possible losing steps for fast image tracking, large volume, and large power consumption for its continuous winding excitation. Because of these disadvantages, voice coil motor (VCM) is one of many promising candidates for next generation digital cameras. The design of an auto-focusing module for a digital camera is thus becomes an engineering challenge because of the optimal integration of mechanical design, electromagnetic design, power IC design, and servo control IC design.

This work was supported by the National Science Council, Taipei, Taiwan, R.O.C. Project no. NSC 96-ET-7-009-002-ET.

The VCM is evolved from the principle of a loudspeaker in vibrating its diaphragm by exciting its voice coil with a controlled current. Therefore, the VCM are used in applications of linear positioning control systems with small control range, such as an optical read/write head of DVD or an auto-focus module of a digital camera. A VCM is composed of a coil and two yoke plates (top and bottom) where permanent magnets are bonded in a fixture. Its operation principle follows the Lorentz force law and it offers the advantages of simple and rigid structure, fast response, no cogging force, no force ripples, and can be controlled with high accuracy.

The VCM for a portable light-weight camera is required to carry the lens from its original lock position to its maximum transverse distance within a specified settling time with minimum power consumption. It is therefore the design goal of a VCM is to achieve the maximum force producing magnetic circuit with minimum space [1]-[3] and at the same time to lower its power dissipation [4]. In additional to the energy saving and minimum volume requirements, fast dynamic response and high accuracy are also required for the positioning control of the VCM module [5]. Therefore, a systematic design procedure is required to optimize the design process which involved with multiple engineering disciplines. In order to achieve this optimization-oriented design goal, an accurate model of the VCM is important both for the motor design and the servo control chip design.

An increase of the winding space will provide more space for the coils with penalty of decreased magnetic flux density. On the other hand, a decrease of the winding space will result higher magnetic flux density but with lower number of coil winding, which means higher exciting current is required. Another design issue resides in how to arrange a fixed volume of the magnet with properly selected ferromagnetic material within a restricted volume to achieve the largest force constant. This paper presents the modeling of a VCM used for the auto-focusing module of a digital camera with a proposed design procedure to optimize its volumetric servo performance for energy saving.

This paper is organized as follows. Section II describes the objective function of magnetic force to be optimized and

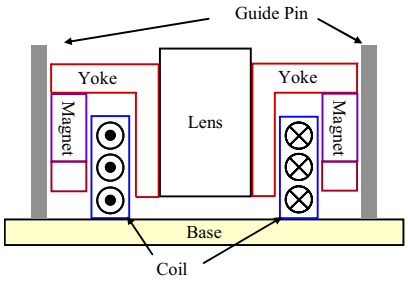

Fig. 1. The structure of the mobile phone camera.

construct the procedure to solve the problem with the aid of Ansoft's Maxwell. Section III derives a mathematical model of the VCM. Section IV shows the comparison of the simulation and experimental results.

II. Magnetic-Field Analysis

Fig. 1 shows the cross-sectional structure of the VCM used for auto-focusing control of the lens for a digital CCD camera and Fig. 2 illustrates its defined design parameters. The permanent magnetic circuit includes a magnet, two yokes, and the air gap. The material of the magnet is NdFeB. Its characteristic equation can be written as $H_c=H_m+B_m/\mu_m$, where H_c represents the coercive force, μ_m is the permeability of the magnet, H_m and B_m are the magnetic field strength and flux density of the magnet, respectively. The material of the yoke is cold-rolled steel. The saturated magnetic flux density B_s of the selected magnet is about 1.3T. In order to achieve maximum usage of the magnetic field and at the same time to maintain a safe tolerance for temperature variation, an empirical value between 85%-90% of its saturated flux density is selected as the designed operating point.

In the permanent magnetic circuit as shown in Fig. 2, the magnitude of the flux density in the air gap

$$\left|\vec{B}_g\right| = \sqrt{H_m B_m \frac{\mu_0 l_m w_1}{l_g y_1 (K_r + 1)}} \tag{1}$$

where

$$K_r = \frac{y_1}{2l_g}\left[\frac{2(R_2 + y_2) - w_1 - w_2}{\mu_{ra} y_2} + \frac{2(Y + w_2) - y_1 - y_2}{\mu_{rb} w_2} + \frac{w_1 + y_1}{\mu_{rc} w_1}\right] \tag{2}$$

If yoke A, yoke B, and yoke C work on the same operation point, their relative permeability $\mu_{ra} = \mu_{rb} = \mu_{rc}$. The VCM's operation principle follows the Lorentz force law

$$\vec{F} = \int_V \vec{J}_c \times \vec{B}_g dV \tag{3}$$

where J_c is the current density and V represents the volume of the coil. The average length per winding l_c is approximately $\pi(2R_1 + 2w_2 + l_g)$. Let B_{gr} be the quantity of $\vec{B}_g$ in the r-direction on the central of the air gap. Assume that the current density is

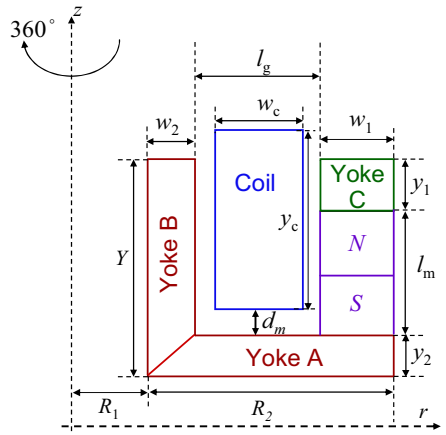

Fig. 2. Definition of geometry parameters.

uniform distributed, and B_{gr} is uniform distribution in the r-direction since the width of the air gap is very small. The magnitude of $\vec{F}$ in the z-direction

$$F_m = i_a \cdot K_F = i_a \cdot \frac{l_g}{D^2} \cdot l_c \cdot \int_{d_m}^{y_c + d_m} B_{gr}(z) dz \tag{4}$$

where i_a is the motor current and D is the diameter of the coil. Let the operation point of the magnet be its maximum energy product that generates larger flux density in the air gap. Enlarging w_1 may increase $\left|\vec{B}_g\right|$, however, if l_g is suppressed, less number of windings are included. Otherwise, if w_2 is suppressed, yoke B may become saturated. Both the conditions decrease K_F. On the other hand, increasing l_m makes yoke A or yoke C become saturated, thus K_r is increased, and $\left|\vec{B}_g\right|$ is decreased.

III. Optimum Design Procedure

Let K_F be the objective function and assume that $y_c = y_1 + l_m$ and the gap between the coil and the yokes is very small, i.e., $l_g \approx w_c$. The optimization problem is described as follows:
Maximize

$$f_{obj} = \frac{l_g}{D^2} \cdot l_c \cdot \int_{d_m}^{y_c + d_m} B_{gr}(z) dz \tag{5}$$

subject to

$$w_1 + w_2 + l_g = R_2 \tag{6}$$

$$y_1 + y_2 + l_m = Y \tag{7}$$

where R_1, R_2 and Y are fixed numbers according to the dimensions specification of the lens module.

The objective function has four independent variables w_1, w_2, y_1 and y_2. If each variable has n possibility, then through out n^4 steps of calculation, one can find the solution. However, this is time consuming. The flow chart that using Ansoft's Maxwell 2D to solve the problem is shown in Fig. 3. The first half of the flow chart is the standard steps to construct a model with

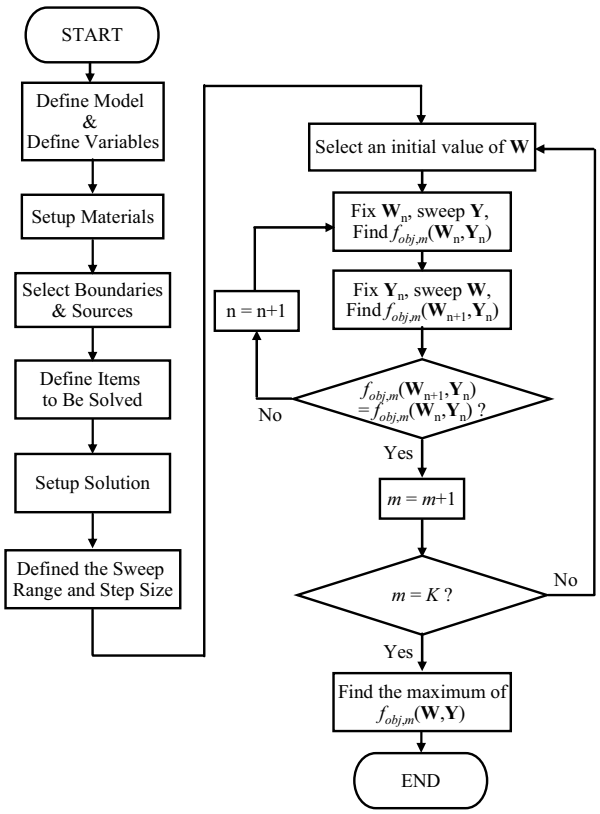

Fig. 3. Flow chart of solving the VCM design optimization problem.

definition of geometric variables. After the environment is set up, let $\mathbf{W} = (w_1, w_2)$ and $\mathbf{Y} = (y_1, y_2)$. Select an initial value of $\mathbf{W}$, named $\mathbf{W_0}$, and sweep $\mathbf{Y}$, until the maximum value of $f_{obj}(\mathbf{Y_0})$ under $\mathbf{W_0}$ is present. Next, fix $\mathbf{Y} = \mathbf{Y_0}$ and sweep $\mathbf{W}$ until the maximum value of $f_{obj}(\mathbf{W_1})$ under $\mathbf{Y_0}$ is present. If the two values of f_{obj} are equal or in the range of calculation error, the solution is converged. Otherwise, the algorithm finds the next value of f_{obj} to compare with the one before.

This method takes much less calculation time than sweep every combination of the four variables. However, it doesn't guarantee to find out the global maximum, thus the outer loop of the flow select K different initial value to compare with one another. Larger K takes more computing resources, and increases the possibility to get the global maximum. Another tip to reduce the computing time is adding the two inequalities: $y_2 \geq w_2$ and $w_1 \geq y_1$, since magnetic flux leakage happens especially at the corner of the L-shaped steel and in the air gap.

Let R_1= 4 mm, R_2= 2 mm, Y= 2.5 mm and the current density J_c= 2.8 A/mm^2. Fig. 4 shows the simulation result of searching $f_{\text{obj,max}}$ using the flow mentioned above. Fig. 4(a) shows that at first, select $\mathbf{Y_0}$ = (0.3, 0.2), sweep $\mathbf{W}$ from (0.05, 0.05) to (0.8, 0.8). The simulation result shows that there exists a local maximum of F_m around $\mathbf{W_0}$ = (0.65, 0.25). This result is definitely to be fixed on the next step since $y_2 < w_2$ is not reasonable.

In Fig. 4 (b), the solution is moved to $\mathbf{W}$= $\mathbf{W_0}$ and $\mathbf{Y_1}$= (0.5, 0.3), the magnetic force is about 26 mN, which is larger than

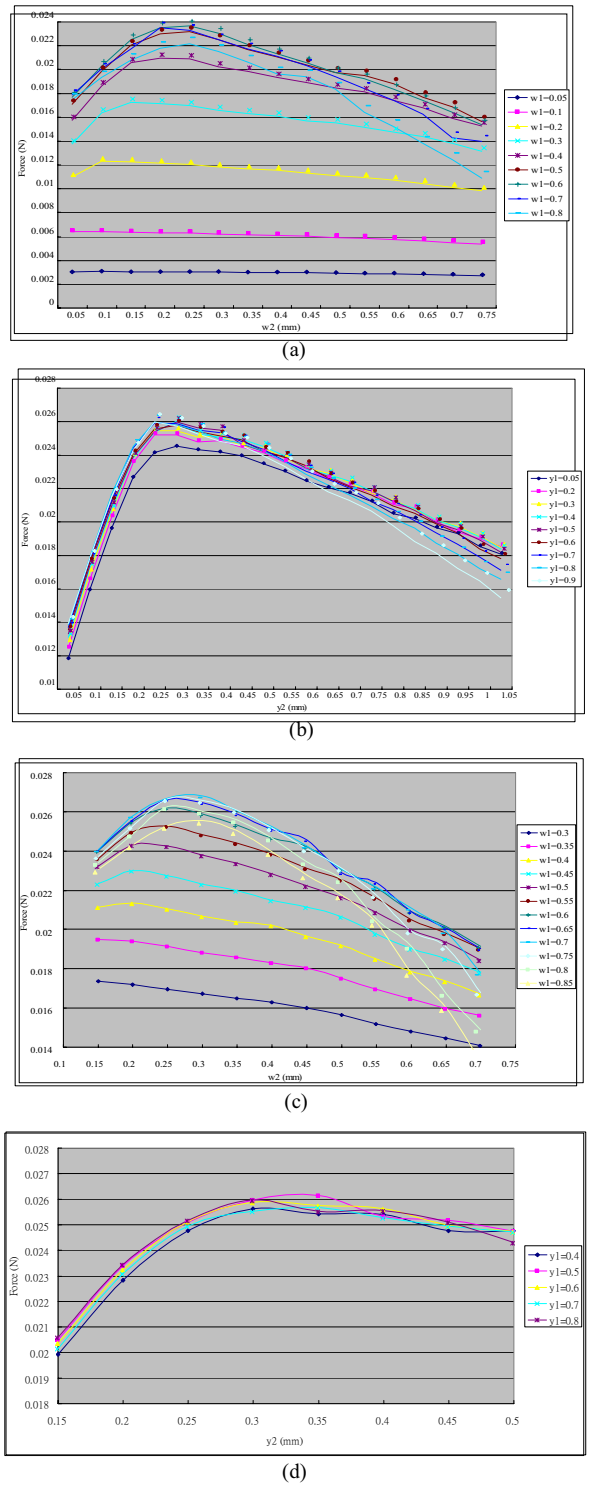

Fig. 4. Searching process for $f_{obj,\max}$; (a) $\mathbf{Y}$=$\mathbf{Y_0}$, search $\mathbf{W}$ for $f_{obj,\max}(\mathbf{W_0},\mathbf{Y_0})$; (b) $\mathbf{W}$=$\mathbf{W_0}$, search $\mathbf{Y}$ for $f_{obj,\max}(\mathbf{W_0},\mathbf{Y_1})$; (c) $\mathbf{Y}$=$\mathbf{Y_1}$, search $\mathbf{W}$ for $f_{obj,\max}(\mathbf{W_1}, \mathbf{Y_1})$; (d) $\mathbf{W}$=$\mathbf{W_1}$, search $\mathbf{Y}$ for $f_{obj,\max}(\mathbf{W_1},\mathbf{Y_2})$.

the one on the first step. It also shows that if y_2 is about 0.2-0.4 mm, increasing y_1 from 0.05 mm to 0.5 mm tends to make more magnetic flux in the r-direction flows throw the air gap,

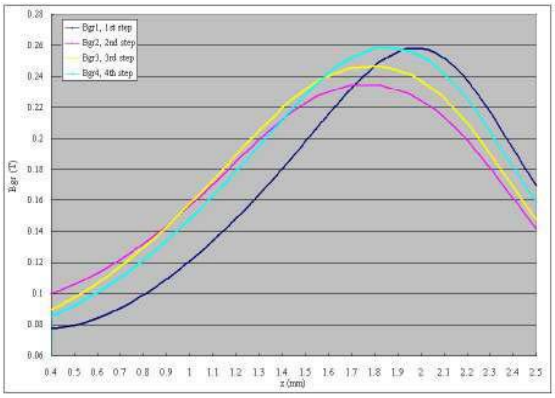

Fig. 5. Comparison of $B_{gr}(z)$ in the air gap of the four steps.

thus enlarge the magnetic force. When l_m is suppressed under 1.2 mm, the flux density in the air gap falls extremely, thus the magnetic force is decreased. If y_1 is fixed, smaller y_2 tends to saturate yoke A and larger y_2 suppress the magnet, thus the maximum value of the magnetic force is in the range of y_2 = 0.2~0.4 mm.

Fig. 4(c) and 4(d) show that the solution is converged around **W**= (0.7, 0.3), **Y**= (0.5, 0.35), and the maximum magnetic force is 26.8 mN with 20 mA motor current, thus the force constant is about 1.34 mN/mA. Compare Fig. 4(a) and 4(c) with Fig. 4(b) and 4(d), it is obvious that the magnetic force varies much more with w_1 than y_1. The reason is that changes in w_1 directly not only affect the flux generate by the permanent magnet, but also the number of windings in the air gap.

To show how the flux density is improved during the optimization process, Fig. 5 illustrates $B_{gr}(z)$ on the central of the air gap of the four steps. Because the initial value of y_1 in the first step is selected very small, the flux density is high in the range of y_1 and the rest part of air gap has low flux density. In the second step, y_1 is increased thus the flux is spread in a wider range. In the next step, w_1 is increased and the permanent magnet generates more flux, thus the flux density in the air gap is increased. Finally, the solution is converged in the fourth step, and the distribution of flux density is B_{r4}.

Fig. 6(a) and 6(b) show the distribution of the flux density and the flux lines, respectively. Since yoke B is a little thinner than yoke A, the magnetic density is about 1.5 T, which is near the magnetic saturation point. If the thermal effect is taken into consideration, it is safer to set w_2= y_2. The flux density is under 1.3 T in yoke A and yoke C, thus no magnetic saturation occurs, the permeability is relatively high.

IV. Modeling of The Lens Module

In a well designed motor, the torque (or force) constant is tuned to be a constant value for its rotating range. However, for a linear motor, especially a mall linear motor with very small transverse distance, limited space, and an aspect ratio close to unity, the resulted force may not be a linear function of the stator current due to a nonlinear flux linkage. According to

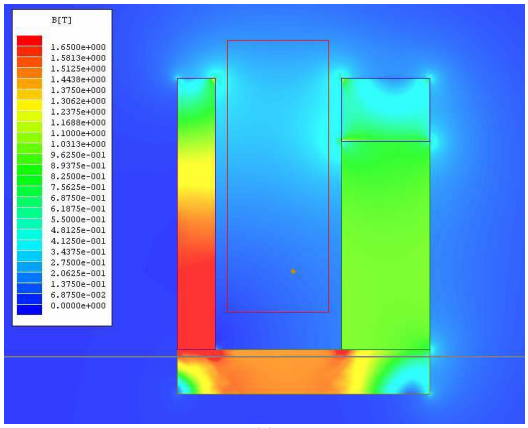

(a)

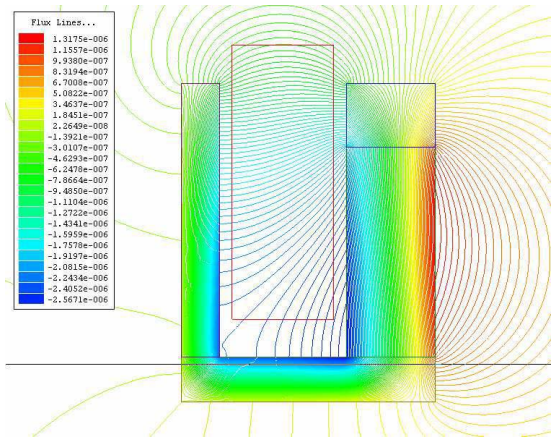

(b)

Fig. 6. (a) The flux density of the optimized permanent magnetic circuit; (b) The flux line of the optimized permanent magnetic circuit.

the design procedure illustrated in the previous section, let B_{r4} be B_{gr} in (4), the force constant K_F is a function of mover position due to the changing coupling field as shown in Fig. 7. The minimum of K_F is 0.128 mN/mA at d_m = 0 mm, and the maximum is 0.952 mN/mA at d_m = 0.43 mm. The average value is 0.63 mN/mA.

The inductance L_a and resistance r_L of the VCM can also be extracted from Maxwell simulation. The conductivity of copper is about 5.8×10^7 siemens/m, thus according to the length of the coil, the resistance of the coil can be calculated. On the other hand, the inductance varies with mover position. When yoke B leaves the coil, the relative permeability of the inductor core is decreased, thus L_a can be represented as a function of d_m. Due to magnetic saturation, L_a also varies with motor current i_a. However, as shown in Fig. 8, the variation of L_a due to i_a is not obvious since i_a is in the range of ±120 mA for this application. It is the mover position that dominates the variation of L_a. The dynamic model of the lens module can be represented as follows:

$$F_m = (M_c + M_L)\frac{du_m}{dt} + f_r(u_m) + F_d \qquad (8)$$

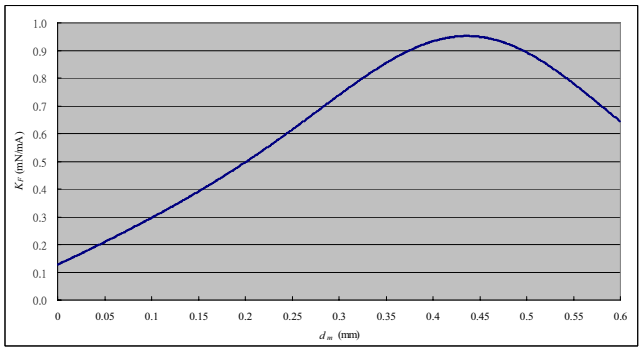

Fig. 7. Simulation derived force constant as a function of mover position.

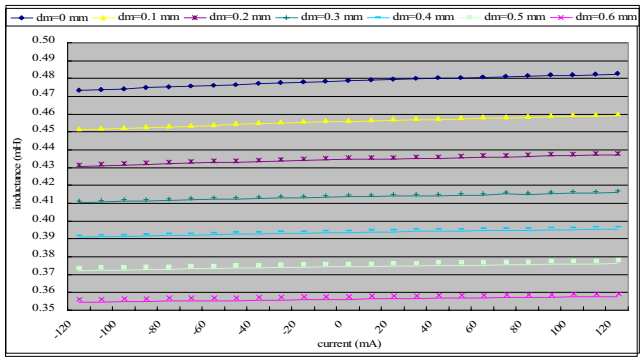

Fig. 8. Calculated coil inductance of the VCM as a function of current and mover position.

$$v_b = u_m \cdot \frac{l_g}{D} \cdot l_c \cdot \int_{d_m}^{y_c+d_m} B_{gr}(z)dz \tag{9}$$

$$v_a - v_b = i_a \cdot r_L + L_a(d_m)\frac{di_a}{dt} \tag{10}$$

where M_c and M_L are the mass of VCM and camera lens, respectively, v_b is the back EMF of the VCM, and u_m is the velocity of the VCM. The variation of L_a due to i_a is ignored in (10).

Fig. 9 shows the block diagram representation of the modeling of the VCM based lens module for auto-focusing. It can be observed that the force constant and coil inductance have been characterized as nonlinear functions of mover position. The force constant reveals a large variation that can not be ignored even with a small range of motion and this is due to the large magnetic force resulted by the stator. The force disturbance comes from the weight of the module. When the module does not move horizontally, the weight of the module should be taken in to consideration. The friction modeling is the standard Coulomb plus static plus viscous friction model [6]-[7]. Let $F_m - F_d$ be F_u and the stick region width be $\pm\Delta u_m$, when the lens is still, $|u_m|<\Delta u_m$:

$$f_r(u_m) = \begin{cases} F_u & if\ |F_u| \le |f_s| \\ f_s \cdot \mathrm{sgn}(F_u) & otherwise \end{cases} \tag{11}$$

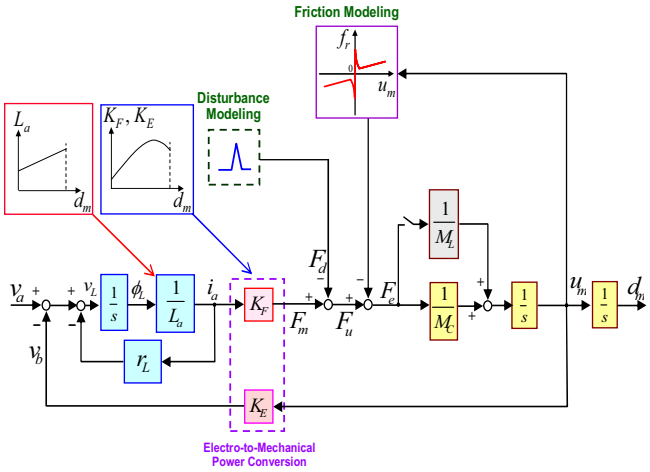

Fig. 9. Block diagram representation of the VCM for auto-focusing.

and when the lens is in motion, $|u_m|>\Delta u_m$:

$$f_r(u_m) = f_c\ \mathrm{sgn}(u_m) + K_B u_m \tag{12}$$

where $f_c > 0$ is Coulomb friction level, f_s is the static friction force, and $K_B > 0$ is the viscous friction coefficient. These parameters are extracted from experiments.

TABLE I
PARAMETERS OF THE TEST VCM

Parameter	Value	Unit
VCM inductor, L	410	mH
ESR of inductor, r_L	25	Ω
force constant, K_F	0.63	mN/mA
back EMF constant, K_E	0.63	V/mm/ms
mass of the VCM, M_C	0.3	g
mass of the lens, M_L	0.7	g
maximum stiction force (with load), f_s	5.9	mN
viscous friction coeff. (with load), K_B	0.082	N/mm/ms

V. EXPERIMENTAL RESULTS

A VCM is constructed based on the proposed design procedure. A position sensor by using a non-contact photo transistor has been designed to convert the physical position 0-0.6 mm to 0.5-1.7 V. In order to verify its performance of the designed VCM and modeling accuracy, a set of sinusoidal voltage waveforms with different frequencies have been applied to the VCM. Fig. 10 shows the closeness of the measured experimental results with the block diagram based simulation results. It should be noted that the motor parameters are derived from the Maxwell 2D - a two-dimensional finite-element based electromagnetic simulation software. It can be also observed that there exists larger error at higher frequency. This may be resulted from parameter error and/or unmodeled high frequency mechanical resonant dynamics. The parameters

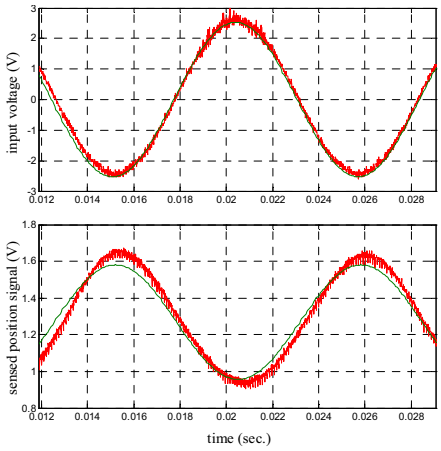

(a)

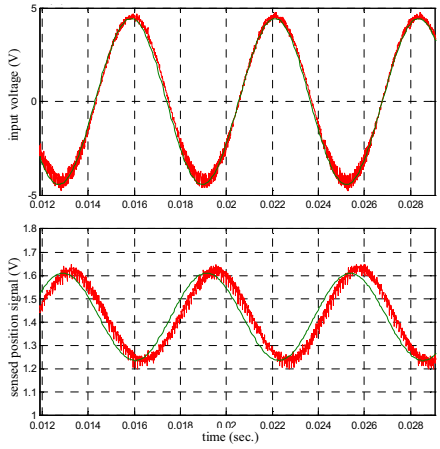

(b)

Fig. 10. Comparison between experimental and simulation results. Input voltage: (a) 94Hz, 2.53V; (b) 160Hz, 4.43V.

of the VCM under test are shown in Table I. Fig. 11 shows that a square wave is applied to the VCM, and the position response of experiment and simulation are consistent.

VI. Conclusion

The VCM used for the auto-focusing of a high-performance slim-type mobile phone must meet the requirements of small size, high accuracy, fast response, and energy saving. The purpose of the magnetic circuit design is to make the VCM achieve maximum force constant under the constraints of limited volume and available current. This paper proposes a systematic method in searching for the maximum value of force constant of the VCM with given design constraints by using an electromagnetic software, the Maxwell 2D of Ansoft. The nonlinear characteristics of the force constant can be derived from the 2D electromagnetic model and be used for the synthesis of its servo controller. The mathematical model of the VCM has been developed and represented by a block diagram with characterized nonlinear elements. A slim-type auto-focusing module with a transverse distance of 0.6 mm has been designed and constructed by using the designed VCM. Simulation results with experimental verification are given to illustrate the proposed design procedure can achieve satisfactory performance.

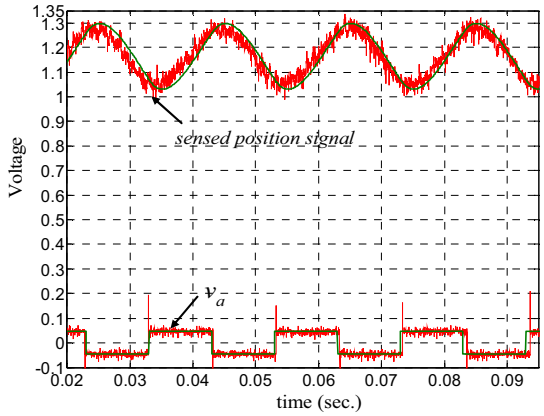

Fig. 11. Comparison between experimental and simulation result. Input square wave: 50Hz, 100 mV.

References

[1] G.P. Widdowson, D. Howe, and P.R. Evison, "Computer-aided optimization of rare-earth permanent magnet actuators," *IEEE Conf. Computation in Electromagnetics*, pp. 93-96, 1991.

[2] L. Encica, J. Makarovic, E.A. Lomonova, and A.J.A Vandenput, "Space mapping optimization of a cylindrical voice coil actuator," *IEEE Conf. Electric Machines and Drives*, pp. 1831-1837, May 2005.

[3] Y.B. Tang, Y.G. Chen, B.H. Teng, H. Fu, H.X. Li, and M.J. Tu, "Design of a permanent magnetic circuit with air gap in a magnetic refrigerator," *IEEE Trans. Magn.*, vol. 40, Issue 3, pp. 1597-1600, May 2004.

[4] Hsing-Cheng Yu, Tzung-Yuan Lee, Shyh-Jier Wang, Mei-Lin Lai, Jau-Jiu Ju, Der-Ray Huang, and Shir-Kuan Lin, "Design of a voice coil motor used in the focusing system of a digital video camera," *IEEE Trans. Magn.*, vol. 41, Issue 10, pp. 3979-3981, Oct. 2005.

[5] B. A. Awaddy, Wu-Chu Shih, and D. M. Auslander, "Nanometer positioning of a linear motion stage under static loads," *IEEE Trans. Mechatronics*, vol. 3, Issue 2, pp. 113-119, June 1988.

[6] Craig T. Johnson and Robert D. Lorenz, "Experimental identification of friction and its compensation in precise, position controlled mechanisms," *IEEE Trans. Industry Applications*, vol. 28, Issue 6, pp. 1392-1398, Nov./Dec. 1992.

[7] Liyu Cao and H. M. Schwartz, "Stick-slip friction compensation for PID position control," *American Control Conference*, vol. 2, pp. 1078-1082, June 2000.